biomass

MDPI

Article

Valorization of Indoor CO_2 into High-Density *Leptolyngbya* sp. Biomass: Spectral Optimization and Continuous Cultivation for Circular Biorefining

Charith Akalanka Dodangodage [1,*], Dhammika Dharmaratne [2], Jagath C. Kasturiarachchi [3] and Rangika Umesh Halwatura [1]

[1] ProGreen Lab, Department of Civil Engineering, University of Moratuwa, Moratuwa 10400, Sri Lanka; rangika@uom.lk
[2] Department of Civil Engineering, Sri Lanka Institute of Information Technology, New Kandy Road, Malabe 10115, Sri Lanka; dhammika.dh@sliit.lk
[3] Department of Applied Sciences, Sri Lanka Institute of Information Technology, New Kandy Road, Malabe 10115, Sri Lanka; jagath.k@sliit.lk
* Correspondence: dodangodageca.24@uom.lk

Abstract

Elevated indoor carbon dioxide (CO_2) represents an underutilized biogenic carbon feedstock. Coupling indoor atmospheric remediation with biological sequestration requires overcoming mass-transfer limitations and culture collapse under high carbon loads. This study empirically evaluated a direct-injection, 2.0 L filamentous *Leptolyngbya* sp. photobioreactor for continuous indoor CO_2 valorization. A fortified nitrogen medium (4.5 g L^{-1} $NaNO_3$) was utilized to sustain high-density proliferation. Initial optimization confirmed that narrow-band Red LEDs (10,000 lux) maximized the Apparent Quantum Efficiency (Φ_{CO_2}) at 1.49 × 10^{-3} mol/mol. During a 20-day continuous trial under 5000 ppm CO_2 sparging, the EPS-rich cyanobacterial matrix resisted acidification, achieving a stationary biomass density of 3.30 g L^{-1}. The system maintained a steady bio-mitigation velocity of ~2120 ppm day^{-1}. Intracellular chlorophyll *a* peaked at 26.0 mg L^{-1} on Day 10, before severe optical self-shading induced a 47% photoprotective degradation, defining Day 10 as the optimal biorefinery harvesting threshold. At this peak, dynamic efficiency reached 2.07 × 10^{-3} mol/mol. Projecting these kinetics onto a 50 m^3 occupied room confirms that capturing ambient CO_2 requires a working volume of 85–90 L and a spatial footprint of <0.25 m^2, validating *Leptolyngbya* sp. as a highly resilient catalyst for decentralized, commercial-scale indoor bioprocessing.

Keywords: *Leptolyngbya* sp.; biomass valorization; circular bioeconomy; biorefinery co-products; photobioreactor scaling; bioenergetic efficiency; carbon dioxide mitigation

Check for updates

Received: 28 July 2026
Revised: 27 August 2026
Accepted: 31 August 2026
Published: 4 September 2026

Copyright: © 2026 by the authors. Licensee MDPI, Basel, Switzerland. This article is an open access article distributed under the terms and conditions of the Creative Commons Attribution (CC BY) license.

1. Introduction

Harnessing phototrophic microorganisms presents a sustainable and circular pathway for biological carbon capture and the concurrent synthesis of renewable bioproducts [1,2]. However, transitioning these biological platforms from high-footprint open ponds to decentralized indoor environments requires a continuous, economical, and concentrated carbon source [3]. Modern architectural envelopes increasingly prioritize thermal energy conservation through airtight construction, which restricts passive air exchange and inadvertently drives anthropogenic carbon dioxide (CO_2) accumulation well beyond baseline atmospheric

thresholds [4,5]. Rather than treating localized indoor CO_2 buildup solely as an environmental hazard linked to Sick Building Syndrome [6], this gas stream represents an abundant, highly accessible biogenic feedstock. Coupling localized indoor atmospheric remediation with phototrophic biosequestration provides a dual-purpose framework within the circular bioeconomy: actively remediating enclosed microclimates while directly valorizing waste gas into dense cellular biomass. Beyond intracellular pigments, cyanobacterial extracellular polymeric substances (EPS) and phycocyanin offer high-value downstream trajectories for sustainable infrastructure, including the development of carbon-negative protective coatings exhibiting high UV stability and adhesion [7,8].

Conventional indoor atmospheric remediation relies heavily on demand-controlled ventilation (DCV) [9]. This strategy mechanically dilutes indoor pollutants by conditioning substantial influxes of outdoor air, creating a severe energetic penalty for the building's HVAC operational load [10,11]. Physicochemical capture technologies—such as solid amine sorbent arrays and direct air capture (DAC) modules—bypass excessive outdoor air dilution but introduce substantial parasitic thermal regeneration penalties [12,13]. Biological sequestration circumvents these intensive thermal regeneration demands because phototrophic microorganisms directly assimilate dissolved inorganic carbon via the Calvin-Benson-Bassham cycle into structural organic polymers [2].

Despite this theoretical advantage, standard indoor biological filtration systems suffer from distinct hydrodynamic and physiological bottlenecks [14]. Most conventional biofilters rely on passive gas–liquid surface diffusion or separate gas-mixing chambers, which severely restrict gas dissolution velocities and induce liquid-phase carbon starvation [15]. To overcome these mass-transfer constraints, photobioreactor architectures must deploy a direct-injection mechanism that delivers CO_2 directly into the liquid culture. However, when conventional unicellular chlorophytes (such as *Chlorella vulgaris* or *Scenedesmus obliquus*) are subjected to direct, elevated carbon spikes (e.g., 5000 ppm), the rapid influx of unbuffered carbonic acid drives severe localized acidification [16]. This pH depression impairs Ribulose-1,5-bisphosphate carboxylase/oxygenase (RuBisCO) activity and frequently triggers culture collapse, limiting the stationary biomass density of typical indoor green microalgal systems to between 1.0 and 2.0 g L^{-1} [17,18].

Filamentous cyanobacteria offer superior structural resilience and photometric flexibility for continuous indoor cultivation. Strains such as *Leptolyngbya* sp. synthesize an intricate sheath of Extracellular Polymeric Substances (EPS) that aggregates cellular trichomes into cohesive mats and provides local pH-buffering capacity against acute carbon spikes [19,20]. Beyond shear and chemical tolerance, cyanobacteria possess specialized extrathylakoidal antenna complexes termed phycobilisomes (PBS), enriched with phycocyanin and allophycocyanin [21]. The PBS architecture allows cyanobacteria to undergo Complementary Chromatic Adaptation (CCA), dynamically reorganizing pigment ratios to optimize photon absorption across distinct wavebands [22]. Because artificial lighting represents the primary operational electrical load in enclosed photobioreactors, matching the narrow-band emission spectrum of light-emitting diodes (LEDs) to the specific absorption bands of *Leptolyngbya* sp. is essential to maximize the Apparent Quantum Efficiency and improve the overall bioprocess energy balance [23].

To establish commercial feasibility, indoor cultivation must be linked with downstream circular biorefining pipelines. While dense biomass accumulation is critical for carbon mass valorization, the progressive optical self-shading that occurs in high-density cultures triggers a documented photoprotective down-regulation of photosynthetic antennae [24,25]. This leads to the degradation of high-value intracellular co-products, particularly chlorophyll *a* and phycobiliproteins. Systematically quantifying the kinetic divergence between gross biomass proliferation and pigment retention is therefore necessary to pinpoint the op-

timal harvesting window that maximizes co-product extraction yields [26]. While artificial illumination represents the primary operational electrical load in enclosed photobioreactors, baseline efficiency metrics remain heavily constrained. Recent literature evaluating artificial lighting for indoor cyanobacterial cultivation generally reports Apparent Quantum Efficiencies (Φ_{CO_2}) hovering between 0.80×10^{-3} and 1.10×10^{-3} mol/mol under standard broad-spectrum white LEDs [21,23]. Precisely quantifying the extent to which narrow-band spectral alignment can exceed these baseline thermodynamic limits—specifically under continuous high-carbon indoor loads—remains a critical gap in optimizing standalone bio-remediation appliances.

To address these engineering and biological knowledge gaps, this investigation empirically quantifies the mass-transfer boundaries, spectro-radiometric efficiency, and long-term metabolic stability of a direct-injection *Leptolyngbya* sp. photobioreactor. The study is driven by the primary hypothesis that spectro-radiometric alignment using narrow-band Red LED arrays matching the primary phycobiliprotein absorption bands will yield a superior Apparent Quantum Efficiency compared to broad-spectrum white illumination. Furthermore, it is hypothesized that the EPS-rich filamentous architecture of *Leptolyngbya* sp. will maintain structural integrity and steady-state carbon uptake under repetitive, direct 5000 ppm CO_2 spikes, achieving stationary biomass densities that exceed standard chlorophyte benchmarks. Ultimately, the core objective is to systematically decouple abiotic dissolution from biological fixation, map the temporal degradation kinetics of intracellular chlorophyll *a*, and determine the precise kinetic parameters required to model and scale appliance-sized indoor air remediation systems for the circular bioeconomy.

2. Materials and Methods

2.1. Cyanobacterial Strain and Pre-Cultivation Standardization

This research employed *Leptolyngbya* sp. (EU310428), a filamentous cyanobacterium sourced from the ProGreen Laboratory culture collection at the University of Moratuwa's Department of Civil Engineering, Moratuwa, Sri Lanka). This specific strain was selected for its robust extracellular polymeric substance (EPS) matrix and its established potential for downstream valorization into bio-based products. The base biomass was cultivated autotrophically in autoclaved BG-11 nutrient broth. Environmental parameters were strictly maintained at 25 ± 2 °C, with an uninterrupted light supply of 150 µmol m^{-2} s^{-1} delivered via cool-white light-emitting diodes.

Because *Leptolyngbya* sp. naturally secretes extracellular polymeric substances (EPS) that bind cells into dense macroscopic mats, conventional pipetting cannot ensure homogeneous volumetric distribution. To overcome this, the pre-cultivation biomass underwent brief mechanical shearing. Agitation with sterile 3 mm glass beads temporarily separated the filaments without inducing cellular lysis. This micro-homogenization process guaranteed a standardized starting density for all experimental phases. Following exponential proliferation, the suspended cells were pelleted by centrifugation at 4000 rpm for 20 min, then integrated into fresh BG-11 medium to achieve the precise target inoculum concentration [27,28].

2.2. Photobioreactor Architecture and Microclimate Control

The macroscopic mass transfer kinetics of the biological matrix were evaluated utilizing a customized, hermetically sealed gas-exchange chamber. The primary external enclosure consisted of a 20.0 L transparent glass vessel. To accurately model human-occupied environments, the internal micro-climate was regulated at 25 ± 1 °C and 60 ± 5% relative humidity, perfectly aligning with ASHRAE Standard 62.1 thermal comfort thresholds [29,30].

A 2.0 L internal photobioreactor (PBR) housing the cyanobacterial suspension (dimensions: 13.0 cm internal diameter, 25.0 cm height) was centrally mounted within this primary vessel (Figure 1). To accurately replicate an acute indoor carbon load and eliminate the kinetic bottlenecks associated with passive headspace transfer, ultra-pure CO_2 gas was directly injected into the cyanobacterial culture via a micro-porous sparger located at the base of the reactor. The off-gas was subsequently vented into the surrounding 20.0 L chamber.

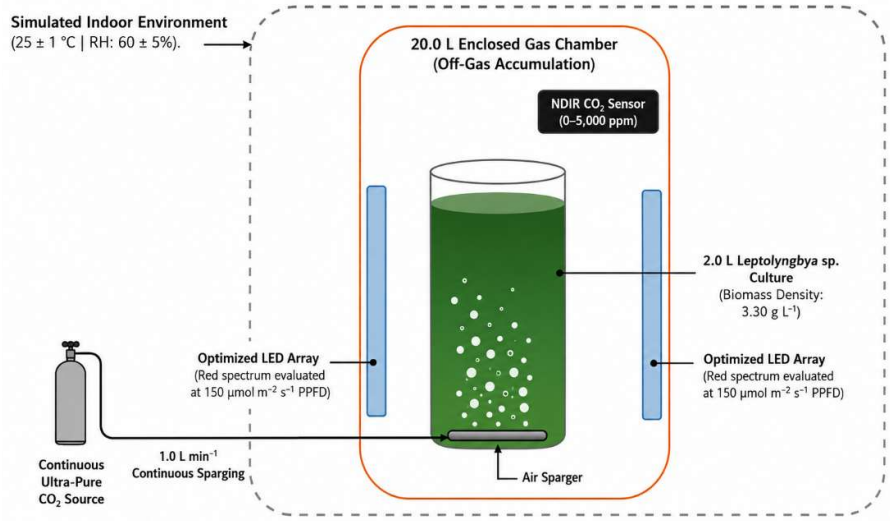


Figure 1. Schematic representation of the 2.0 L direct-injection photobioreactor system. The diagram illustrates the continuous CO_2 sparging mechanism, the optimized narrow-band Red LED array, and the 20.0 L enclosed off-gas accumulation chamber utilized for continuous bio-mitigation monitoring within a simulated indoor microclimate.

The hydrodynamic profile was stabilized by locking the aeration rate at 1.0 L min^{-1}, corresponding to 0.5 volumes of air per volume of liquid per minute (vvm). This configuration sustained a uniform superficial gas velocity (U_g), ensuring robust cell-to-gas contact while preventing biomass sedimentation and boundary-layer stagnation. Real-time atmospheric metrics of the system's off-gas—specifically temperature, humidity, and the CO_2 decay profile—were monitored using an integrated Non-Dispersive Infrared (NDIR) detector (Sper Scientific, Model 800050, Scottsdale, AZ, USA). This sensor features a functional span of 0–5000 ppm and a certified precision tolerance of ±50 ppm plus 3% of the absolute reading [31,32]. To preserve strict experimental sterility, all chamber components and PBR surfaces were sanitized with a 70% ethanol solution before every trial. Furthermore, to prevent instrument drift, the NDIR module was subjected to a weekly two-point recalibration protocol utilizing atmospheric air and a validated 5000 ppm standard calibration gas.

2.3. Abiotic Gas Dissolution and Physical Calibration

Accurately quantifying biogenic carbon capture requires the mathematical separation of active metabolic fixation from passive gas dissolution. Consequently, an initial abiotic calibration procedure was conducted to map the baseline physical mass-transfer characteristics of the uninoculated hardware. The central 2.0 L PBR was charged with pure, sterile BG-11 medium, and dosed with the direct 5000 ppm CO_2 injection. While maintaining the standard 25 °C environment and continuous 0.5 vvm aeration, the off-gas CO_2 depletion was logged every 10 min over a complete 24-h cycle. The resulting abiotic dissolution curve established the absolute physical boundary of the aeration matrix acting upon a Newtonian fluid [33]. This empirical baseline was subsequently subtracted from the raw biological data to isolate the true kinetic rate of *Leptolyngbya* sp. carbon assimilation [30,31].

2.4. Phase 1: Optical Parameter Optimization and Kinetic Screening

Prior to the extended longevity trials, a targeted screening matrix was executed to isolate the most energetically efficient spectro-radiometric conditions for the cyanobacterial catalyst. To guarantee rheological consistency, the 2.0 L PBR was populated with a standardized initial biomass density of 0.30 g L^{-1} for each independent biological triplicate [31,34].

The testing framework manipulated two primary physical variables: specific emission spectra and luminous intensity. Four distinct lighting arrays (cool-white, red, blue, and green LEDs) were positioned symmetrically at a 5.0 cm radial offset from the reactor wall to ensure homogeneous light distribution. Prior to initiation, the spectral power distribution and surface illuminance were rigorously mapped using a calibrated quantum spectroradiometer (LI-COR Biosciences, Lincoln, NE, USA). Each discrete color spectrum was evaluated across an intensity gradient of 2500, 5000, 10,000, and 15,000 lux, yielding an approximate Photosynthetically Active Radiation (PAR) range of 35 to 210 µmol m^{-2} s^{-1}.

Every batch run commenced with a direct 5000 ppm CO_2 injection into the culture, followed by 24 h of continuous kinetic tracking. To eliminate carbon memory effects and accumulated physiological fatigue, the entire apparatus was purged with standard atmospheric air and refilled with a freshly cultivated biomass aliquot between each trial. The specific combination of color and intensity that maximized both the absolute CO_2 assimilation velocity and the Apparent Quantum Efficiency (Φ_{CO_2}) was mathematically defined as the operational setpoint for Phase 2 [35–37].

2.5. Phase 2: Extended Operational Stability and Cyclic Carbon Loading

Upon identifying the optimal lighting parameters, a prolonged twenty-day cultivation phase was executed. This stage aimed to evaluate the structural stability, functional consistency, and long-term metabolic endurance of the *Leptolyngbya* sp. biomass under continuous carbon stress [31,35]. The photobioreactor was freshly inoculated and maintained strictly under the ideal spectro-radiometric conditions established during Phase 1.

To sustain high-density proliferation and prevent premature nitrogen starvation under continuous high-carbon loading, the standard BG-11 medium was modified prior to inoculation. Specifically, the formulation was amended with a 3-fold concentration of sodium nitrate ($NaNO_3$, 4.5 g L^{-1}), providing an expanded elemental nitrogen ceiling mathematically capable of supporting a theoretical biomass threshold exceeding 4.0 g L^{-1}.

The system operated under a continuous 24:0 h (light/dark) photoperiod to evaluate the maximum volumetric biomass productivity and the continuous bioprocessing capacity of the cyanobacterial matrix, uninfluenced by natural day-night cycles. Throughout this duration, a rigorous and repetitive carbon-loading protocol was enforced. Specifically, the culture was directly spiked to a peak CO_2 concentration of 5000 ppm every 24 h. This extended testing phase yielded the longitudinal carbon fixation and biomass accumulation data required to accurately model the cyanobacterial matrix's growth kinetics and operational lifespan [37,38].

2.6. Analytical Procedures for Cellular and Pigment Quantification

To accurately track the physiological status and biokinetic efficiency of the filamentous cells under repetitive CO_2 loading, discrete 5.0 mL culture aliquots were extracted strictly every 24 h at 10:00 AM. This rigid 24-h sampling frequency ensured a standardized metabolic integration window between discrete atmospheric carbon spikes, eliminating temporal bias prior to downstream quantitative analysis.

2.6.1. Gravimetric Biomass Assessment

Biomass accumulation was measured gravimetrically as dry cell weight (DCW). Because *Leptolyngbya* sp. naturally forms highly entangled filamentous networks, an immediate, high-frequency mechanical micro-homogenization step was applied to all samples prior to extraction. This procedure guaranteed a uniform, representative suspension for analysis.

Pre-weighed, moisture-free glass microfiber filters (Hyundai GF/C, 1.2 µm pore size, 47 mm diameter, Seoul, Republic of Korea) were used to filter specific volumes of the homogenized culture. The biomass-laden filters were subsequently placed in a thermostatic oven at 60 °C and dried until they reached a constant mass. To avoid ambient moisture reabsorption, the filters were transferred to a desiccator to cool before the final weighing. The ultimate biomass concentrations were calculated utilizing the following formula [34,39]:

$$DCW_n = \frac{W_f - W_i}{V}$$

where DCW_n is the biomass concentration at sampling day n (g L^{-1}), W_f is the final mass of the dried filter plus retained biomass (g), W_i is the initial mass of the dried filter (g), and V is the filtered sample volume (L).

2.6.2. Chlorophyll *a* Recovery and Analysis

To evaluate the resilience of the photosynthetic apparatus and overall pigment vitality against constant CO_2 saturation, the concentration of intracellular chlorophyll *a* was closely monitored. The extraction procedure involved treating the harvested cell pellets with 10 mL of 100% pure acetone, allowing the solvent to effectively penetrate the cyanobacterial cells. To maximize pigment recovery and prevent light-induced degradation, this suspension was incubated at 4 °C in total darkness for 24 h.

Following the dark incubation, the samples were centrifuged at 3500× *g* for 10 min to pellet the cellular debris. The clarified supernatant containing the extracted pigments was collected, and its optical absorbance was measured using a spectrophotometer at 662 nm and 750 nm. The 750 nm reading served as a baseline correction for any residual sample turbidity. Standardized empirical equations [40] were applied to these corrected values to determine the final chlorophyll *a* concentrations, serving as a primary indicator of physiological stress across the twenty-day trial, as well as quantifying the accumulation of a high-value intracellular co-product targeted for downstream biorefinery extraction.

2.7. Bioenergetic Calculations and Reactor Efficiency Metrics

To assess the photon utilization efficiency of *Leptolyngbya* sp. and mathematically identify the most efficient illumination profile, the Apparent Quantum Efficiency (Φ_{CO_2}) was computed for every evaluated optical condition. The general procedure required a three-step mathematical conversion: first, transforming raw photometric lux into biologically relevant photosynthetic photon flux density (PPFD); second, mapping this irradiance to the internal geometry of the reactor to define the volumetric incident photon flux; and finally, establishing the ratio between the continuous molar carbon assimilation rate and the total photon supply.

2.7.1. Calculation of Photosynthetic Photon Flux Density

Standard photometric illuminance (lux) is heavily biased toward human ocular sensitivity rather than the true photosynthetic action spectrum. Consequently, baseline lux readings were transformed into absolute Photosynthetic Photon Flux Density (PPFD, µmol m^{-2} s^{-1}) utilizing precise spectral conversion factors (CF_λ) derived directly from

the quantum spectroradiometer's absolute power distribution. This approach rigorously quantifies the actual biophysically relevant photon supply:

$$PPFD = E_v \times CF_\lambda$$

where E_v is the measured illuminance (lux) and CF_λ represents the spectrum-specific conversion factor tailored to the individual LED array emissions.

2.7.2. Determination of Reactor-Scale Photon Exposure (I_{abs})

The total photo-energy penetrating the biological matrix, defined as the volumetric incident photon flux (I_{abs}, expressed in mol m^{-3} s^{-1}), was calculated by mapping the PPFD over the illuminated geometry of the internal chamber [41,42]:

$$I_{abs} = \frac{PPFD \times A_{illuminated}}{V_{PBR}} \times 10^{-6}$$

where $A_{illuminated}$ is the radial surface area of the PBR exposed to the LED arrays (0.080 m^2), V_{PBR} is the working volume of the cyanobacterial suspension (2.0×10^{-3} m^3), and 10^{-6} is the conversion constant from micromoles (µmol) to moles (mol).

2.7.3. Quantification of Net Biological Carbon Fixation (R_{CO_2})

The active biological carbon assimilation rate was isolated by subtracting the established abiotic physical mass transfer baseline from the steady-state gas CO_2 differential. Because the reactor operates under continuous direct-injection sparging rather than as a static closed batch, the absolute molar rate of CO_2 fixation (R_{CO_2}, expressed in mol L^{-1} day^{-1}) was derived using the continuous gas flow rate and the Ideal Gas Law [42,43]:

$$R_{CO_2} = \frac{\Delta C_{bio} \times 10^{-6} \times Q \times P}{R \times T \times V_{PBR}}$$

where ΔC_{bio} is the steady-state bio-mediated CO_2 depletion differential (ppm), Q is the continuous volumetric gas flow rate (1440 L day^{-1}), P is the atmospheric pressure (1 atm), R is the ideal gas constant (0.0821 L atm K^{-1} mol^{-1}), T is the absolute ambient temperature (298.15 K), V_{PBR} is the working liquid volume of the cyanobacterial suspension (2.0 L), and 10^{-6} is the conversion factor from parts-per-million volume fraction to dimensionless molar fraction.

2.7.4. Calculation of Apparent Photon Conversion Efficiency (Φ_{CO_2})

Finally, the photon utilization efficiency of the biological matrix under varying light spectra was quantified by calculating the Apparent Photon Utilization Efficiency [42,43]. This metric represents the moles of CO_2 assimilated per mole of incident photons supplied [44,45]:

$$\Phi_{CO_2} = \frac{R_{CO_2}}{I_{abs}}$$

The spectro-radiometric combination yielding the highest Φ_{CO_2} value was analytically designated as the most energy-efficient setpoint, dictating the operational parameters for the longitudinal Phase 2 trials.

2.8. Data Processing and Statistical Evaluation

To ensure rigorous reproducibility, all experimental protocols were performed in independent biological triplicates (n = 3). Replicate batches were fully randomized to eliminate potential spatial or temporal clustering biases. Data sets are reported as the

mean ± standard deviation (SD). Visualization of all kinetic and growth profiles was executed exclusively using Microsoft Excel (Microsoft Corporation, Redmond, WA, USA).

A full factorial Design of Experiments (DOE) was not deployed because the primary objective was to isolate the independent physiological responses to specific, pre-determined LED wavebands rather than modeling complex multi-variable interactions. Consequently, all statistical evaluations were processed using Minitab 17 (Minitab, LLC, State College, PA, USA). The fundamental assumptions of data normality and homoscedasticity were confirmed via the Shapiro–Wilk and Levene's tests, respectively. A two-way analysis of variance (ANOVA) was deployed to model the isolated and synergistic impacts of the varying emission spectra and illuminance levels during Phase 1. When statistically significant variations were detected, Tukey's Honestly Significant Difference (HSD) post hoc test was executed to isolate discrete pairwise deviations, with statistical significance firmly established at $p < 0.05$.

3. Results

3.1. Quantification of Abiotic Mass Transport Boundaries and System Calibration

Before analyzing the photosynthetic capacity of the *Leptolyngbya* sp. culture, it was necessary to map the strictly physical gas–liquid mass transfer constraints of the 2.0 L reactor. This baseline calibration ensures that biological CO_2 uptake is mathematically isolated from the passive dissolution of carbon gas into the uninoculated BG-11 fluid. Operating the continuous mechanical sparging system at 0.5 vvm (1.0 L min^{-1}) generated a superficial gas velocity (U_g) of roughly 1.75×10^{-3} m s^{-1}.

During the preliminary 24-h abiotic calibration, injecting a continuous 5000 ppm CO_2 gas stream produced a stabilization profile governed completely by the gas–liquid concentration gradient. The uninoculated BG-11 medium reached steady-state carbon saturation rapidly. After equilibrium was established, the continuous exhaust stream stabilized at 4630 ± 110 ppm. Consequently, the maximum physical carbon depletion driven purely by abiotic dissolution was established at a steady differential of 370 ± 14 ppm, representing a 7.4% decrease from the 5000 ppm inlet load. Throughout all temporal checkpoints and independent replicates (n = 3), standard deviations were tightly maintained within 2–5% of the average recorded values (Figure 2).

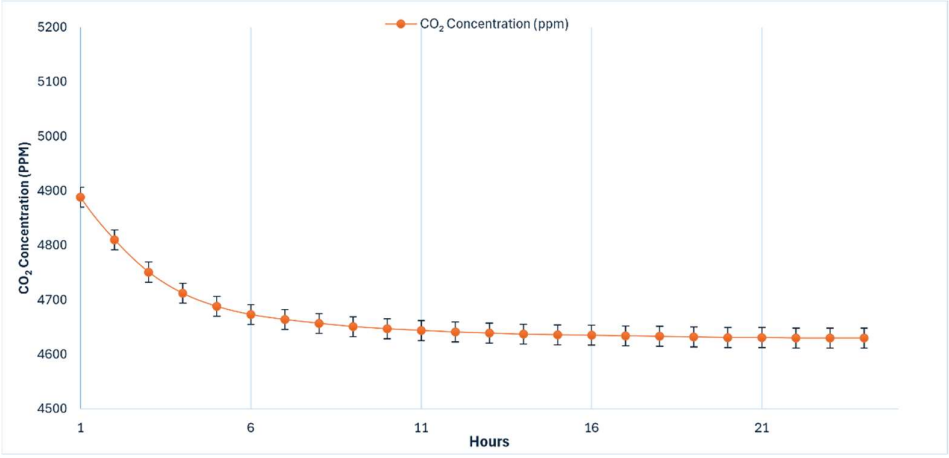


Figure 2. Non-biological 24-h transient CO_2 decay profile determining the equilibrium saturation threshold of sterile BG-11 medium (n = 3).

To confirm that this physical baseline would hold steady throughout the prolonged timeline mandated for Phase 2, an extended 20-day abiotic longevity trial was conducted. Under continuous 5000 ppm sparging, the physical mass transfer boundaries proved

highly consistent, logging an average continuous abiotic CO_2 dissolution differential of 387.6 ± 13.5 ppm (Figure 3). This low variance confirms the mechanical reliability of the aeration hardware, proving that daily operations do not induce saturation drift. For all ensuing biological trials, this specific abiotic diffusion limit was systematically deducted from the gross CO_2 concentration measurements. Therefore, any carbon reduction measured beyond this threshold is exclusively credited to the active photobiological assimilation mechanisms of the *Leptolyngbya* sp. matrix.

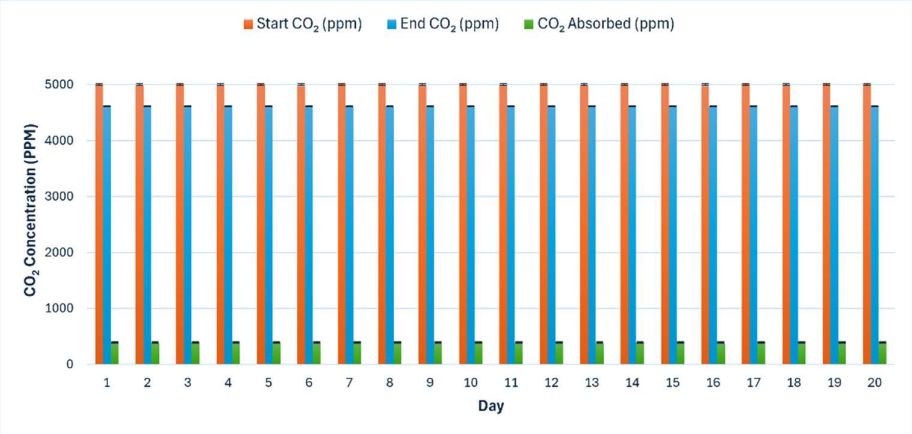


Figure 3. Extended 20-day evaluation of abiotic CO_2 dissolution stability under repeated daily injections of 5000 ppm (n = 3).

3.2. Phase 1: Influence of Optical Parameters on Carbon Assimilation Dynamics

Once the abiotic mass transfer constraints were defined, Phase 1 proceeded to measure the macroscopic carbon fixation kinetics generated by the *Leptolyngbya* sp. catalyst. To determine the absolute bio-mediated assimilation rates, the raw exhaust depletion data was mathematically corrected by subtracting the established 370 ppm physical dissolution baseline.

3.2.1. Impact of Illuminance Levels

Initially, the cyanobacterial system was exposed to a gradient of light intensities (2500, 5000, 10,000, and 15,000 lux) utilizing White LEDs to pinpoint the onset of photosynthetic saturation. The empirical data outlined a positive, non-linear relationship between incident photon supply and CO_2 removal. Operating at the minimum tested intensity of 2500 lux yielded a gross steady-state differential of 1270 ± 58 ppm, translating to a net biological carbon fixation of 900 ppm.

Carbon assimilation velocity accelerated as illuminance escalated ($p < 0.05$). The 10,000 lux setting drove a highly efficient assimilation profile, drawing the 5000 ppm continuous inlet load down to an exhaust concentration of 2880 ppm. This corresponds to a gross atmospheric reduction of 2120 ± 82 ppm, leaving a net bio-mediated assimilation of 1750 ppm. Pushing the intensity higher to 15,000 lux resulted in a gross depletion of 2300 ± 95 ppm (net 1930 ppm), but these marginal gains signaled the beginning of photosystem saturation and diminishing metabolic efficiency. As a result, the 10,000 lux threshold was analytically selected as the optimal baseline for spectral evaluation (Figure 4).

3.2.2. Influence of Emission Spectra

To gauge how spectral quality dictates carbon fixation efficiency, the cyanobacterial matrix was illuminated using distinct LED wavebands (Red, Blue, Green, and White) fixed at the 10,000 lux optimum. The resulting kinetic profiles varied heavily depending on the supplied optical spectrum.

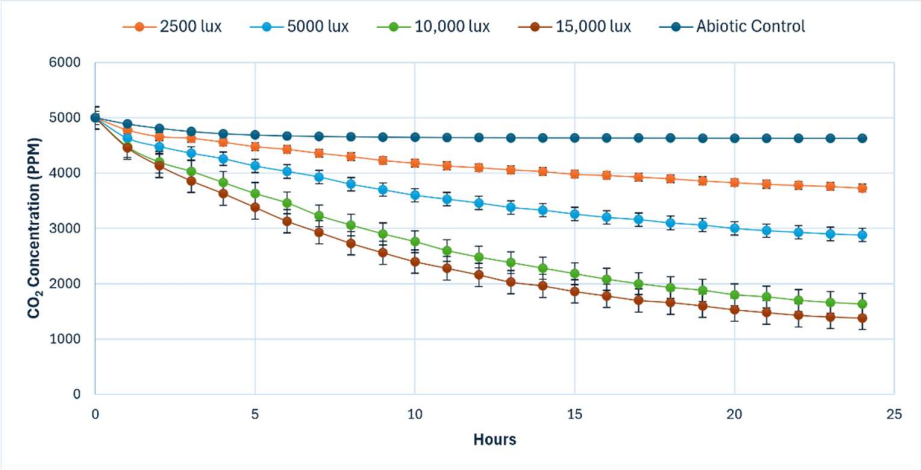


Figure 4. Kinetic CO_2 decay profiles from Phase 1, illustrating biological performance across varying irradiance limits over a 24-h cycle (n = 3).

The *Leptolyngbya* sp. culture demonstrated superior assimilation kinetics under the narrow-band Red LED array. The red spectrum drove the 5000 ppm CO_2 inlet load down to a steady-state exhaust of 2230 ppm. This gross depletion differential of 2770 $\pm$ 95 ppm (representing a net biological assimilation of 2400 ppm) significantly outpaced both the standard White LED control (gross depletion: 2120 $\pm$ 82 ppm, $p < 0.05$) and the Blue LED array (gross depletion: 1570 $\pm$ 65 ppm, $p < 0.05$).

In contrast, the Green LED spectrum triggered a severe drop in conversion efficiency. Gross CO_2 depletion under green light plateaued at just 600 $\pm$ 32 ppm. After accounting for the abiotic baseline, the absolute biological assimilation was merely 230 ppm, constituting an 88.7% decline in photobiological effectiveness when benchmarked against the red spectrum ($p < 0.05$). These assimilation metrics provide the fundamental mathematical justification for deploying the Red spectrum at 10,000 lux as the primary operational configuration for the Phase 2 longitudinal stability trials (Figure 5).

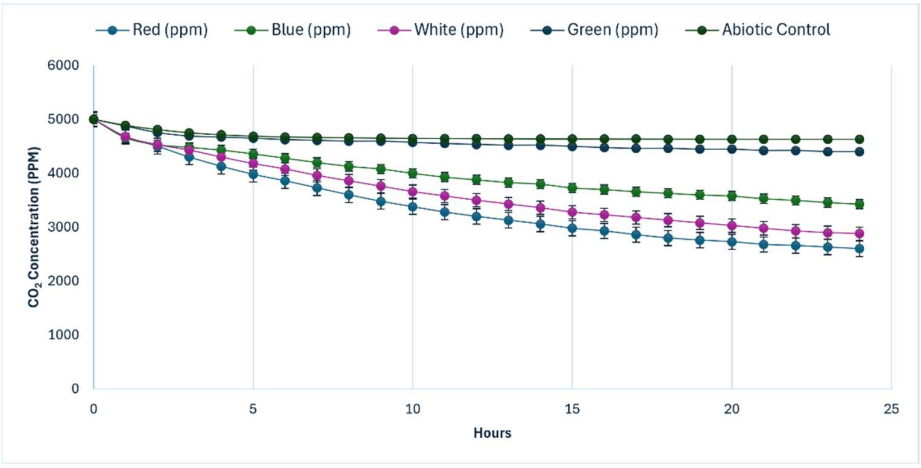


Figure 5. Phase 1 kinetic CO_2 depletion curves evaluating discrete spectral wavelengths over 24 h (n = 3).

3.3. Phase 2: Extended Bioprocess Stability and Continuous Carbon Fixation

To determine the prolonged functional durability of the biomass-generation system, the *Leptolyngbya* sp. biomass underwent a twenty-day continuous endurance trial. The operational environment was locked to the optimized Phase 1 settings (Red LED array at 10,000 lux), and the system was subjected to a continuous 5000 ppm

CO_2 feed. The long-term carbon capture profile was characterized by three distinct kinetic stages: initial metabolic adjustment, maximum assimilation velocity, and ultimate steady-state equilibrium.

3.3.1. Initial Adjustment and Maximum Assimilation Velocity (Days 1–11)

Over the first three days of acclimation, the photobioreactor maintained a stable baseline, achieving a mean gross CO_2 reduction of 2658 ± 95 ppm. Proceeding past Day 3, assimilation rates surged as the cyanobacterial network fully adapted to the high-concentration carbon load. Peak system efficiency occurred on Day 10, logging an absolute gross reduction differential of 3725 ± 142 ppm. By factoring out the specific 404 ppm abiotic baseline recorded for that day, the peak biological fixation was calculated at 3321 ppm. Throughout this high-efficiency window (Days 7–11), the biologically active *Leptolyngbya* sp. successfully sequestered more than 65% of the continuous 5000 ppm CO_2 inlet load.

3.3.2. Biomass Densification and Steady-State Equilibrium (Days 12–20)

Following Day 11, the carbon fixation profile exhibited a controlled decline. Gross CO_2 reduction decreased from 3410 ± 128 ppm on Day 12 down to 2650 ± 105 ppm by Day 15 (Figure 6). This kinetic drop is a highly predictable bioprocess consequence: as the filamentous network proliferates heavily, optical self-shading occurs, restricting the volumetric incident photon flux (I_{abs}) capable of penetrating the radial core of the reactor.

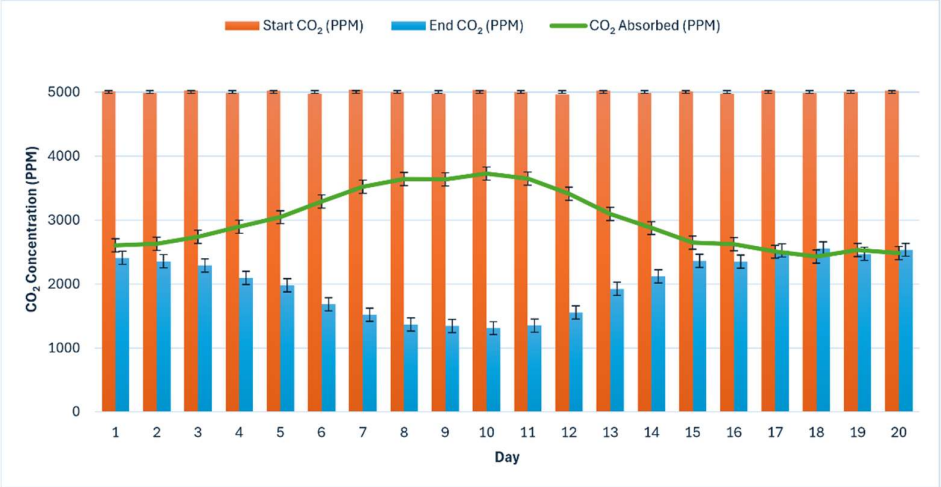


Figure 6. Extended 20-day CO_2 mitigation profile of the *Leptolyngbya* sp. matrix operating under the optimized Red LED (10,000 lux) parameters. The red curve illustrates the gross daily CO_2 sequestration (n = 3).

Even under severe optical limitation, the biological matrix resisted structural failure. Between Days 16 and 20, the *Leptolyngbya* sp. system transitioned into a stable operational plateau, with gross carbon depletion leveling out at a consistent 2515 ± 98 ppm. When adjusted for abiotic diffusion, the continuous biological sequestration rate stabilized at 2120 ppm. This sustained equilibrium confirms the operational resilience of the continuous bioprocessing system.

3.4. Extended Biomass Accumulation and Intracellular Pigment Dynamics

Daily assessments of dry cell weight (DCW) and intracellular chlorophyll *a* levels were conducted to confirm the biological vitality and physical durability of the *Leptolyngbya* sp. culture.

3.4.1. Gravimetric Cellular Proliferation

Originating from a normalized baseline density of 0.30 ± 0.01 g L^{-1}, the culture's growth dynamics followed a classic sigmoidal pattern under high-carbon stress. The primary metabolic adjustment window (Days 1–3) yielded minor cellular multiplication, reaching 0.40 ± 0.02 g L^{-1}. Beginning on Day 4, the cyanobacteria transitioned into rapid exponential proliferation, fully exploiting the continuous CO_2 supply and the fortified nitrogen medium. Cellular mass surged from 0.75 ± 0.03 g L^{-1} on the fourth day to 3.00 ± 0.12 g L^{-1} by Day 11. Between Days 15 and 20, the entangled filamentous network plateaued into a stable stationary state, narrowly resting between 3.28 ± 0.14 and 3.31 ± 0.15 g L^{-1} (Figure 7).

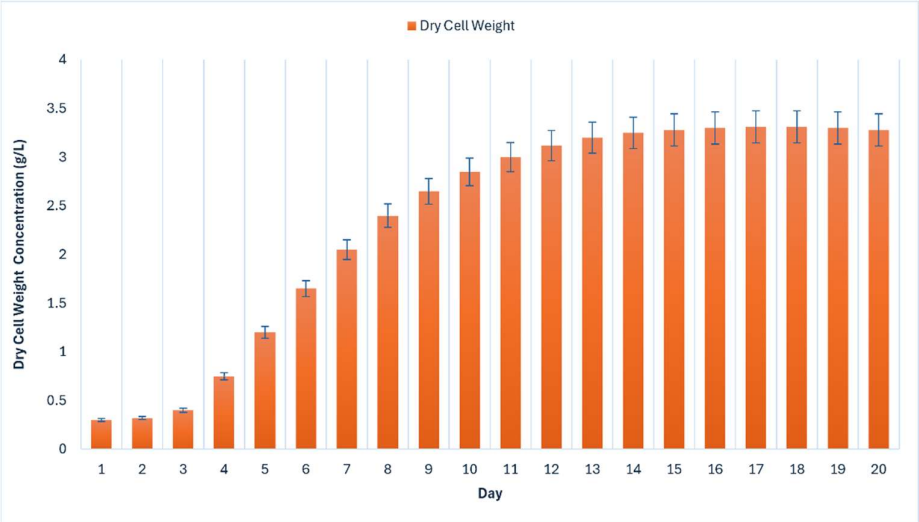


Figure 7. Continuous 20-day evaluation of cellular proliferation quantified via Dry Cell Weight (DCW) (n = 3).

3.4.2. Intracellular Pigment Evolution

The temporal profile of intracellular chlorophyll *a* disconnected completely from the overall biomass trajectory during the experiment's final phase. Synthesis of this valuable biorefinery co-product surged alongside early cellular replication, climbing from a baseline of 1.3 ± 0.05 mg L^{-1} to an absolute maximum of 26.0 ± 1.1 mg L^{-1} by Day 10. Notably, this biochemical zenith coincides exactly with the highest gross carbon reduction observed on that day (Figure 8).

In stark contrast, as the reactor density shifted into the stationary plateau (exceeding a DCW of 3.0 g L^{-1}), pigment generation collapsed. Beginning on Day 11 and continuing through Day 20 (13.7 ± 0.6 mg L^{-1}), chlorophyll *a* concentrations experienced a steep, linear decline. Crucially, this 47% decrease from the Day 10 maximum did not precipitate a corresponding drop in cellular mass; the overall DCW remained consistent at ~3.30 g L^{-1}. For downstream biorefining applications, this characterization dictates that biomass must be harvested prior to this stationary phase to maximize the recovery of high-value co-products.

3.5. Bioenergetic Analysis and Reactor-Scale Photon Utilization

The empirical kinetic data were converted into macroscopic reactor efficiency indicators utilizing the continuous steady-state volumetric equations defined in Section 2.7. Initial photometric lux measurements were transformed into Photosynthetic Photon Flux Density (PPFD) utilizing precise spectral power conversions.

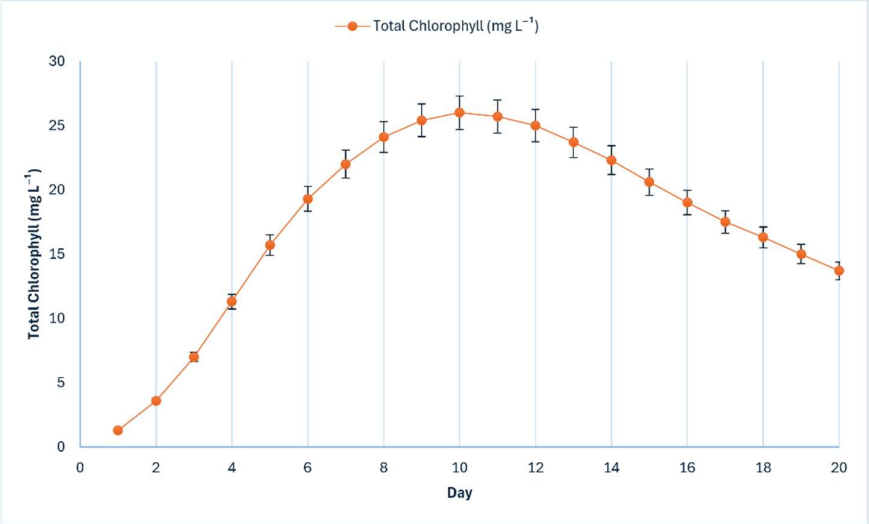


Figure 8. 20-day temporal progression of intracellular chlorophyll *a* concentrations (n = 3).

3.5.1. Phase 1: Irradiance Saturation Thresholds

While scaling illuminance produced a linear rise in volumetric incident photon flux, the corresponding Apparent Quantum Efficiency (Φ_{CO_2}) displayed a negative correlation. Operating at 2500 lux yielded the greatest photon conversion efficiency (2.83×10^{-3} mol/mol). Advancing to 10,000 lux provided (Table 1) the optimal energetic compromise, driving robust volumetric carbon fixation while preserving strong utilization efficiency (1.38×10^{-3} mol/mol) (Table 1).

Table 1. Reactor-level photon utilization efficiencies across varying Phase 1 irradiance intensities.

Intensity (lux)	PPFD	R_{CO_2}	(Φ_{CO_2})
2500	37.5 ± 1.1	0.42 ± 0.02	2.83 ± 0.11 [a]
5000	75.0 ± 2.2	0.66 ± 0.03	2.71 ± 0.10 [a]
10,000 (Selected condition)	150.0 ± 4.5	0.83 ± 0.06	1.38 ± 0.06 [b]
15,000	225.0 ± 6.7	0.91 ± 0.07	1.01 ± 0.05 [c]

Note: Data presented as mean ± SD (n = 3). Superscript letters indicate statistically significant differences ($p < 0.05$) evaluated via one-way ANOVA and Tukey's HSD.

3.5.2. Phase 1: Spectral Waveband Optimization

Following intensity optimization, the system was subjected to discrete spectral wavelengths at the fixed 10,000 lux setpoint. Integrating the empirical conversion factors and continuous ΔC differentials confirmed the Red emission spectrum as the optimal condition. Under red illumination, the Apparent Quantum Efficiency reached 1.49×10^{-3} mol/mol, driving a mathematically superior absolute carbon assimilation rate compared to the White control (Table 2).

3.5.3. Phase 2: Temporal Evolution of System Efficiency

Maintaining the Red LED parameters over the 20-day cultivation period revealed that photon utilization efficiency is highly dynamic. On Day 10, the system achieved its highest measured dynamic efficiency, recording an Apparent Quantum Efficiency of 2.07×10^{-3} mol/mol—a substantial increase over the initial Phase 1 baseline. By Day 20, as optical self-shading took full effect, the efficiency mathematically plateaued at 1.32×10^{-3} mol/mol (Table 3).

Table 2. Spectro-radiometric carbon-capture efficiencies of *Leptolyngbya* sp. at the 10,000 lux baseline.

Light Spectrum	PPFD	R_{CO_2}	(Φ_{CO_2})
Red (Selected condition)	190.0 ± 5.7	1.13 ± 0.03	1.49 ± 0.06 [a]
White	150.0 ± 4.5	0.83 ± 0.02	1.38 ± 0.06 [b]
Blue	210.0 ± 6.3	0.57 ± 0.02	0.68 ± 0.03 [c]
Green	120.0 ± 3.6	0.11 ± 0.01	0.23 ± 0.01 [d]

Note: Data presented as mean ± SD (n = 3). Superscript letters indicate statistically significant differences ($p < 0.05$).

Table 3. Temporal variation in Apparent Quantum Efficiency (AQE) (Φ_{CO_2}) across the 20-day Phase 2 longitudinal stress trial (Red LED, 10,000 lux).

Phase 2 Milestone	Net CO_2 Assimilation (ppm Day^{-1})	R_{CO_2} ($\times 10^{-5}$ mol m^{-3} s^{-1})	Φ_{CO_2} ($\times 10^{-3}$ mol/mol)
Day 1 (Acclimation)	2260	1.07 ± 0.03	1.41 ± 0.05
Day 10 (Peak Velocity)	3321	1.57 ± 0.05	2.07 ± 0.08
Day 20 (Steady-State)	2090	1.00 ± 0.03	1.32 ± 0.05

Note: Data presented as mean ± SD (n = 3).

4. Discussion

4.1. Spectro-Radiometric Optimization and Phycobilisome Excitation Dynamics

The spectro-radiometric screening in Phase 1 demonstrated that narrow-band Red LED illumination delivered the highest Apparent Quantum Efficiency ($\Phi_{CO_2} = 1.49 \times 10^{-3}$ mol/mol) for the *Leptolyngbya* sp. matrix, outperforming both broad-spectrum White and monochromatic Blue configurations. This photonic response is intrinsically governed by the specialized light-harvesting architecture of cyanobacteria. Unlike eukaryotic green microalgae, which rely predominantly on membrane-bound chlorophyll-protein complexes, cyanobacteria utilize extrathylakoidal antenna complexes termed phycobilisomes (PBS). The core and rod sub-elements of PBS—primarily composed of phycocyanin ($\lambda_{max} \approx 620$ nm) and allophycocyanin ($\lambda_{max} \approx 650$ nm)—exhibit maximum optical absorption within the red waveband, facilitating efficient excitation energy transfer directly into the reaction centers of Photosystem II [21].

While cyanobacteria possess the capacity for Complementary Chromatic Adaptation (CCA) to alter internal pigment stoichiometry under shifting light environments [46,47], the Blue LED array yielded a markedly lower reactor-scale photon efficiency ($\Phi_{CO_2} = 0.68 \times 10^{-3}$ mol/mol). Under blue wavelengths, a substantial fraction of absorbed photons is intercepted by non-photosynthetic carotenoids or dissipated as non-photochemical quenching, creating a suboptimal ratio of total photon capture to carbon reduction chemistry [48,49]. Furthermore, the severe kinetic suppression observed under Green LEDs ($\Phi_{CO_2} = 0.23 \times 10^{-3}$ mol/mol) confirms that green photons largely bypass the primary absorption bands of this strain's PBS rods. Selecting narrow-band Red illumination aligns photon delivery with the biological absorption spectrum, maximizing volumetric carbon fixation rates ($R_{CO_2} = 1.13 \times 10^{-5}$ mol m^{-3} s^{-1}) while minimizing wasted electrical irradiance [23].

4.2. Extended Operational Endurance, Photoprotective Down-Regulation, and Matrix Resilience

Long-term bioprocess stability requires physiological adaptation to continuous high-carbon saturation. Over the 20-day Phase 2 endurance trial, the *Leptolyngbya* sp. culture maintained steady biological carbon assimilation (~2120 ppm day^{-1}) despite a

47% reduction in intracellular chlorophyll *a* after Day 10. In dense phototrophic suspensions, such pigment attenuation is a well-documented physiological response to optical self-shading [24,25]. As dry cell weight approached the stationary plateau (3.30 g L^{-1}), the elevated cellular packing density increased light attenuation across the radial profile of the reactor. By down-regulating peripheral chlorophyll antennae, the outer cell layers mitigated photo-oxidative stress and reactive oxygen species (ROS) formation, while facilitating deeper photon penetration into the reactor core [26].

The structural persistence of the culture under repetitive 5000 ppm CO_2 dosing is directly attributable to its filamentous morphology and protective extracellular polymeric substance (EPS) matrix. The dense EPS sheath acts as a physical and chemical buffer, mitigating localized pH swings caused by carbonic acid formation during direct gas sparging [19,20]. This protective barrier prevented the cellular lysis and auto-flocculation that frequently destabilize unicellular microalgae under severe carbon loading [50,51], confirming *Leptolyngbya* sp. as an exceptionally robust catalyst for continuous indoor bioprocessing.

4.3. Kinetic Benchmarking Against Contemporary Biological Platforms

Juxtaposing the performance of the *Leptolyngbya* sp. photobioreactor against published indoor air remediation and carbon capture systems highlights significant kinetic advantages. The majority of bench-scale indoor biofilters deploy single-celled chlorophytes, such as *Chlorella vulgaris* or *Scenedesmus obliquus*, operated under ambient atmospheric conditions (~400 ppm CO_2). These eukaryotic systems typically achieve stationary biomass densities between 1.0 and 2.0 g L^{-1} and exhibit carbon removal velocities rarely exceeding 800–1200 ppm day^{-1} [17,18]. Furthermore, when exposed to sudden, elevated CO_2 spikes, unicellular chlorophytes often suffer from kinetic inhibition due to unbuffered medium acidification, which impairs Ribulose-1,5-bisphosphate carboxylase/oxygenase (RuBisCO) activity [16,52].

In contrast, the direct-injection *Leptolyngbya* sp. system achieved a stationary biomass density of 3.30 g L^{-1}—representing a 1.6- to 3.3-fold increase over conventional indoor chlorophyte platforms [17,18]. The peak biological fixation velocity recorded on Day 10 (3321 ppm day^{-1}) and the steady-state mitigation rate (~2120 ppm day^{-1}) significantly exceed the continuous performance of compact microalgal reactors documented in the recent literature [18,53]. This performance is driven by the synergistic combination of direct-injection gas–liquid mass transfer, spectral matching via PBS antennae, and the pH-buffering capacity of the cyanobacterial EPS matrix [20,21]. Furthermore, integrating continuous indoor atmospheric remediation with zero-dilution, waste-to-resource platforms allows for simultaneous high-density biomass accumulation and the recovery of circular bioeconomy co-products [54].

4.4. Architectural Scale-Up Modeling, Appliance Footprint, and Auxiliary Integration

To bridge the gap between bench-scale kinetics and practical built-environment deployment, the empirical mass-transfer rates must be projected onto a standard architectural scenario [14,55]. As commercial architecture rapidly adopts zero-waste frameworks—utilizing upcycled industrial waste for high-performance thermal insulation and ceiling composites [56]—the integration of active biological air-polishing appliances provides a necessary atmospheric counterbalance for these highly sealed environments.

Applying the true continuous volumetric carbon fixation rate demonstrated by the *Leptolyngbya* sp. reactor under steady-state direct-injection operation ($R_{CO_2} = 0.062$ mol L^{-1} day^{-1}):

$$V_{req} = \frac{\text{Daily Human Metabolic } CO_2 \text{ Output (mol day}^{-1})}{\text{Volumetric Fixation Rate (mol L}^{-1}\text{ day}^{-1})}$$

For an 8-h occupancy period generating roughly 6.1 mol of CO_2, maintaining ambient concentrations below the ASHRAE 1000 ppm threshold requires an active culture working volume (V_{req}) of approximately 98.4 L. Structuring this 100 L volume into a modular, flat-panel or annular vertical array (e.g., thickness: 0.10 m, height: 1.50 m, width: 0.66 m) yields a total physical equipment footprint of just 0.066 m^2 of floor area, easily satisfying spatial constraints for indoor deployment.

To function reliably as a standalone indoor appliance, the biological reactor must integrate dedicated auxiliary systems [57,58]:

- Direct-Injection Aeration: A low-noise, variable-speed diaphragm sparging pump (1.0–1.5 vvm) coupled to fine-bubble micro-porous diffusers to ensure optimal gas residence time.
- Optoelectronic Array: A high-efficiency Red LED array ($\lambda \approx 660$ nm) delivering 150–190 µmol m^{-2} s^{-1} PPFD, mounted with passive heat sinks to prevent thermal transfer to the culture.
- Atmospheric & Process Control: An integrated NDIR CO_2/RH/temperature sensor module connected to an automated feedback controller to modulate sparging velocity based on real-time room occupancy.
- HVAC Coupling: Inlet and exhaust manifolds designed to connect directly into the dedicated return-air plenum of local fan coil units, enabling continuous air polishing without imposing parasitic drag on the building's central air handling unit [9].

4.5. Downstream Biorefinery Trajectories and Operational Constraints

Establishing economic viability within a circular bioeconomy requires coupling indoor carbon abatement with high-value co-product recovery [1,2]. The kinetic decoupling between dry cell weight (3.30 g L^{-1}) and chlorophyll *a* content (13.7 mg L^{-1} at Day 20 vs. 26.0 mg L^{-1} at Day 10) establishes a definitive operational guideline: operating in a continuous batch mode past Day 10 degrades high-value pigment yields by 47%. Consequently, commercial systems should implement a semi-continuous turbidostat harvesting regime, maintaining biomass density near 3.0 g L^{-1} by periodic harvesting to maximize both volumetric carbon mitigation and the extraction of high-value pigments (chlorophyll *a* and C-phycocyanin) [24,53]. Following optimal harvesting, the recovered biomass can be further processed or subjected to targeted metabolic shifts to generate functionally enhanced, phytotoxicity-free bio-fertilizer feedstocks for sustainable agriculture [59,60].

A primary engineering constraint identified in continuous indoor photobioreactors is the electrical power required for continuous artificial illumination [57,61]. Future iterations must explore high-frequency pulsed LED illumination synchronized with the millisecond turnover kinetics of Photosystem II reaction centers, which can reduce parasitic lighting power loads by 30–50% without compromising biomass productivity [23,62]. Additionally, while pure CO_2 was utilized here for kinetic precision, authentic indoor microclimates contain complex mixtures of volatile organic compounds (VOCs) and particulates, necessitating long-term field validation under authentic occupant loading conditions [8,57].

5. Conclusions

This study validates the structural and kinetic superiority of a direct-injection *Leptolyngbya* sp. photobioreactor for continuous indoor CO_2 abatement and biomass valorization. By transitioning from passive diffusion models to continuous gas sparging, this system overcomes traditional mass-transfer bottlenecks. Spectro-radiometric optimization confirmed that aligning narrow-band Red LED emission with cyanobacterial phycobilisomes significantly maximizes Apparent Quantum Efficiency (Φ_{CO_2}), peaking dynamically at 2.07×10^{-3} mol/mol.

Subjected to continuous 5000 ppm CO_2 dosing, the EPS-rich filamentous matrix actively buffered localized acidification, completely preventing the culture collapse typical of indoor chlorophyte systems. Supported by nitrogen fortification, the matrix achieved a stationary density of 3.30 g L^{-1} and a steady-state continuous mitigation rate of ~2120 ppm day^{-1}. The 47% drop in intracellular chlorophyll *a* following Day 10 defines the absolute temporal boundary for commercial harvesting to maximize high-value biorefinery yields prior to optical self-shading.

Architectural scale-up calculations prove that maintaining standard indoor microclimates below ASHRAE thresholds can be accomplished using an 85–90 L modular appliance requiring less than 0.25 m^2 of floor space. Subsequent engineering efforts must prioritize high-frequency pulsed LED illumination to minimize the parasitic electrical load, paving the way for commercially viable, decentralized circular biorefining.

Author Contributions: Conceptualization, C.A.D.; methodology, C.A.D.; validation, C.A.D.; formal analysis, C.A.D.; investigation, C.A.D.; resources, C.A.D. and R.U.H.; data curation, C.A.D.; writing—original draft preparation, C.A.D.; writing—review and editing, J.C.K., D.D. and R.U.H.; visualization, C.A.D.; supervision, J.C.K. and R.U.H.; project administration, R.U.H. All authors have read and agreed to the published version of the manuscript.

Funding: This research received no external funding.

Data Availability Statement: The raw data supporting the conclusions of this article will be made available by the authors on request.

Acknowledgments: The authors wish to acknowledge the Kalana Mithuro organization for their support during this research. We also thank the technical officers W. B. U. Rukma, D. M. B. Wickramasinghe, U. K. Padmaperuma, and T. P. D. G. I. Yohan for their technical assistance, and W. J. Shantha for his support in the laboratory. During the preparation of this work, the authors utilized Google Gemini (Google LLC) for advanced language polishing, grammatical refinement, and structural formatting assistance. Additionally, ChatGPT-5.5 (OpenAI) was utilized to assist in the conceptual design and graphic rendering of the reactor schematic (Figure 1). Following the use of these tools, the authors thoroughly reviewed, heavily edited, and validated all generated content. The authors assume full responsibility and ultimate accountability for the scientific integrity, accuracy, and originality of the final manuscript.

Conflicts of Interest: The authors declare no conflicts of interest.

References

1. Abdur Razzak, S.; Bahar, K.; Islam, K.M.O.; Haniffa, A.K.; Faruque, M.O.; Hossain, S.M.Z.; Hossain, M.M. Microalgae cultivation in photobioreactors: Sustainable solutions for a greener future. *Green Chem. Eng.* **2024**, *5*, 418–439. [CrossRef]
2. Alkhamis, Y.A.; Mathew, R.T.; Nagarajan, G.; Rahman, S.M.; Rahman, M.M. pH induced stress enhances lipid accumulation in microalgae grown under mixotrophic and autotrophic condition. *Front. Energy Res.* **2022**, *10*, 1033068. [CrossRef]
3. An, K.; Li, K.; Yang, C.M.; Brechtl, J.; Nawaz, K. A comprehensive review on regeneration strategies for direct air capture. *J. CO_2 Util.* **2023**, *76*, 102587. [CrossRef]
4. Arora, R.; Sudhakar, K.; Rana, R.S. Photobioreactors for building integration: A overview of designs and architectural potential. *Heliyon* **2024**, *10*, e35168. [CrossRef] [PubMed]

5. *ANSI/ASHRAE Standard 62.1-2010*; Ventilation for Acceptable Indoor Air Quality. American Society of Heating, Refrigerating and Air-Conditioning Engineers: Atlanta, GA, USA, 2010.
6. Atta, M.; Idris, A.; Bukhari, A.; Wahidin, S. Intensity of blue LED light: A potential stimulus for biomass and lipid content in fresh water microalgae Chlorella vulgaris. *Bioresour. Technol.* **2013**, *148*, 373–378. [CrossRef] [PubMed]
7. Borella, L.; Marchese, D.; Trivellin, N.; Sforza, E. Complementary chromatic adaptation as a strategy to increase energy conversion efficiency of microalgae-cyanobacteria consortia in continuous LED photobioreactors. *Energy Convers. Manag.* **2023**, *294*, 117549. [CrossRef]
8. Campbell, D. Complementary chromatic adaptation alters photosynthetic strategies in the cyanobacterium Calothrix. *Microbiology* **1996**, *142*, 1255–1263. [CrossRef] [PubMed]
9. Carvalho, A.P.; Meireles, L.A.; Malcata, F.X. Microalgal reactors: A review of enclosed system designs and performances. *Biotechnol. Prog.* **2006**, *22*, 1490–1506. [CrossRef] [PubMed]
10. Cordoba-Perez, M.; de Lasa, H. CO_2-Derived Carbon Capture and Photon Absorption Efficiency by Microalgae in Novel PhotoBioCREC. *Ind. Eng. Chem. Res.* **2020**, *59*, 14710–14716. [CrossRef]
11. Dange, P.; Gawas, S.; Pandit, S.; Mekuto, L.; Gupta, P.K.; Shanmugam, P.; Kanupriya; Patil, R.; Banerjee, S. Trends in photobioreactor technology for microalgal biomass production along with wastewater treatment: Bottlenecks and breakthroughs. In *An Integration of Phycoremediation Processes in Wastewater Treatment*; Elsevier: Amsterdam, The Netherlands, 2021; pp. 135–154. [CrossRef]
12. Dauchet, J.; Cornet, J.F.; Gros, F.; Roudet, M.; Dussap, C.G. Photobioreactor Modeling and Radiative Transfer Analysis for Engineering Purposes. In *Advances in Chemical Engineering*; Elsevier: Amsterdam, The Netherlands, 2016; Volume 48, pp. 1–106. [CrossRef]
13. Dodangodage, C.A.; Kasturiarachchi, J.C.; Perera, T.A.; Rajapakshe, S.D.; Niyangoda, S.S.; Halwatura, R.U. Sustainable bioremediation of undiluted matured compost leachate and enhanced lipid partitioning in *Desmodesmus* sp.: A zero-dilution approach for circular bioeconomy. *Front. Microbiol.* **2026**, *17*, 1872485. [CrossRef]
14. Dodangodage, C.A.; Kasturiarachchi, J.C.; Perera, T.A.; Rajapakshe, S.D.; Niyangoda, S.S.; Halwatura, R.U. Biochemical shifts in *Chlorella vulgaris* via post-stationary magnesium sulfate stress: Optimizing biomass for advanced bio-fertilizers. *Front. Plant Sci.* **2026**, *17*, 1867866. [CrossRef] [PubMed]
15. Dodangodage, C.A.; Premarathne, H.; Kasturiarachchi, J.C.; Perera, T.A.; Rajapakshe, D.; Halwatura, R.U. Algae-Based Protective Coatings for Sustainable Infrastructure: A Novel Framework Linking Material Chemistry, Techno-Economics, and Environmental Functionality. *Phycology* **2025**, *5*, 84. [CrossRef]
16. Dodangodage, C.A.; Gamage, G.N.; Halwatura, R.H.; Kasturiarachchi, J.C.; Perera, T.A.; Rajapakshe, S.D.; Niyangoda, S.S.; Halwatura, R.U. Circular valorization of acid-hydrolyzed fishery wastewater: Integrated remediation and enhanced C-phycocyanin production by *Spirulina* sp. *Front. Environ. Sci.* **2026**, *14*, 1816065. [CrossRef]
17. Dodangodage, C.A.; Gamage, G.N.; Mallawa, L.C.; Kasturiarachchi, J.C.; Fernando, K.V.; Halwatura, R.H.; Perera, T.A.; Rajapakshe, S.D.; Niyangoda, S.S.; Halwatura, R.U. Production of Carbohydrate-Rich *Chlorella* sp. Biomass Using Clarified Aquaponics Effluent for Bioethanol Feedstock Applications. *Biomass* **2026**, *6*, 26. [CrossRef]
18. Dodangodage, C.A.; Gamage, G.N.; Wijesekara, I.A.; Kasturiarachchi, J.C.; Perera, T.A.; Rajapakshe, D.; Halwatura, R.U. Valorization of Canteen Wastewater Through Optimized Spirulina Platensis Cultivation for Enhanced Carotenoid Production and Nutrient Removal. *Phycology* **2026**, *6*, 15. [CrossRef]
19. Dodangodage, C.A.; Kasturiarachchi, J.C.; Wijesekara, I.A.; Perera, T.A.; Rajapakshe, D.; Halwatura, R. Integrated Microalgal–Aquaponic Systems for Enhanced Water Treatment and Food Security: A Critical Review of Recent Advances in Process Integration and Resource Recovery. *Phycology* **2026**, *6*, 14. [CrossRef]
20. Dodangodage, C.A.; Rathnapriya, R.H.N.S.; Gamage, G.N.; Kasturiarachchi, J.C.; Perera, T.A.; Rajapakshe, S.D.; Niyangoda, S.S.; Halwatura, R.U. Valorization of acid-hydrolyzed tea stem waste for sustainable biodiesel production using Chlorella vulgaris: A biorefinery approach. *Front. Bioeng. Biotechnol.* **2026**, *14*, 1816002. [CrossRef] [PubMed]
21. Fernando, K.V.; Dodangodage, C.A.; Seneviratne, V.M.; Jayasinghe, S.M.; Dharmaratne, D.; Gamage, G.N.; Halwatura, R.H.; Gunasekera, U.S.W.; Halwatura, R.U. Circular Valorization of Post-Industrial Textile Waste in Thermal-Insulating Cementitious Ceiling Sheets. *Textiles* **2026**, *6*, 27. [CrossRef]
22. Gabrielyan, D.A.; Gabel, B.V.; Sinetova, M.A.; Gabrielian, A.K.; Markelova, A.G.; Shcherbakova, N.V.; Los, D.A. Optimization of CO_2 Supply for the Intensive Cultivation of Chlorella sorokiniana IPPAS C-1 in the Laboratory and Pilot-Scale Flat-Panel Photobioreactors. *Life* **2022**, *12*, 1469. [CrossRef] [PubMed]
23. Gao, Y.; Bernard, O.; Fanesi, A.; Perré, P.; Lopes, F. The effect of light intensity on microalgae biofilm structures and physiology under continuous illumination. *Sci. Rep.* **2024**, *14*, 50432. [CrossRef] [PubMed]
24. Grossman, A.R. A molecular understanding of complementary chromatic adaptation. In *Discoveries in Photosynthesis*; Springer: Dordrecht, The Netherlands, 2005; pp. 959–967. [CrossRef]

25. Hamilton, T.L.; Klatt, J.M.; de Beer, D.; Macalady, J.L. Cyanobacterial photosynthesis under sulfidic conditions: Insights from the isolate *Leptolyngbya* sp. strain hensonii. *ISME J.* **2018**, *12*, 568–584. [CrossRef] [PubMed]
26. Han, M.; Park, J.; Kim, I.; Yi, H. A Microalgae Photobioreactor System for Indoor Air Remediation: Empirical Examination of the CO_2 Absorption Performance of *Spirulina maxima* in a $NaHCO_3$-Reduced Medium. *Appl. Sci.* **2023**, *13*, 12991. [CrossRef]
27. Hou, C.; Zhao, J.; Huang, B.; Zhou, X.; Zhang, Y. Microalgae-based technologies for carbon neutralization and pollutant remediation: A comprehensive and systematic review. *Resour. Conserv. Recycl.* **2024**, *202*, 107323. [CrossRef]
28. Ibrahim, Y.; Kershaw, T.; Shepherd, P.; Coley, D. On the optimisation of urban form design, energy consumption and outdoor thermal comfort using a parametric workflow in a hot arid zone. *Energies* **2021**, *14*, 4026. [CrossRef]
29. Jui, T.J.; Tasnim, A.; Islam, S.M.R.; Manjur, O.H.B.; Hossain, M.S.; Tasnim, N.; Karmakar, D.; Hasan, M.R.; Karim, M.R. Optimal growth conditions to enhance Chlorella vulgaris biomass production in indoor phyto tank and quality assessment of feed and culture stock. *Heliyon* **2024**, *10*, e31900. [CrossRef] [PubMed]
30. Kehoe, D.M.; Grossman, A.R. Complementary chromatic adaptation: Photoperception to gene regulation. *Semin. Cell Biol.* **1994**, *5*, 303–313. [CrossRef] [PubMed]
31. Kim, K.H.; Parrow, M.W.; Kheirkhah Sangdeh, P. Microalgae-integrated building enclosures: A nature-based solution for carbon sequestration. *Front. Built Environ.* **2025**, *11*, 1574582. [CrossRef]
32. Komkhum, T.; Winterburn, J.; Wongsirichot, P.; Janpum, C.; In-Na, P. Microalgal photobioreactors as living air purifiers for better indoor carbon dioxide quality control. *Biomass Bioenergy* **2026**, *211*, 109178. [CrossRef]
33. Li, B.; Cai, W. A novel CO_2-based demand-controlled ventilation strategy to limit the spread of COVID-19 in the indoor environment. *Build. Environ.* **2022**, *219*, 109232. [CrossRef] [PubMed]
34. Lichtenthaler, H.K. Chlorophylls and carotenoids: Pigments of photosynthetic membranes. *Methods Enzymol.* **1987**, *148*, 350–383. [CrossRef]
35. Majhi, B.K. Carbon capture, storage, and utilization in cyanobacteria. *Carbon Resour. Convers.* **2026**, *9*, 100388. [CrossRef]
36. Maltsev, Y.; Maltseva, K.; Kulikovskiy, M.; Maltseva, S. Influence of light conditions on microalgae growth and content of lipids, carotenoids, and fatty acid composition. *Biology* **2021**, *10*, 1060. [CrossRef] [PubMed]
37. Mattos, E.R.; Singh, M.; Cabrera, M.L.; Das, K.C. Effects of Inoculum Physiological Stage on the Growth Characteristics of *Chlorella sorokiniana* Cultivated Under Different CO_2 Concentrations. *Appl. Biochem. Biotechnol.* **2012**, *168*, 519–530. [CrossRef] [PubMed]
38. McQuiston, F.C.; Parker, J.D.; Spitler, J.D.; Taherian, H. *Heating, Ventilating, and Air Conditioning: Analysis and Design*; John Wiley & Sons: Hoboken, NJ, USA, 2023.
39. Mesburis, R.; Rutherford, M.; Handschy, A.V.; Day, D.A.; Morris, M.A.; Ziola, A.C.; Peng, Z.; de Gouw, J.A.; Jimenez, J.L. Mitigation of Indoor Air Pollution from Air Cleaners Using a Catalyst. *ACS ES&T Air* **2025**, *2*, 1694–1703. [CrossRef]
40. Metsoviti, M.N.; Papapolymerou, G.; Karapanagiotidis, I.T.; Katsoulas, N. Effect of light intensity and quality on growth rate and composition of *Chlorella vulgaris*. *Plants* **2020**, *9*, 31. [CrossRef] [PubMed]
41. Mulders, K.J.M.; Lamers, P.P.; Martens, D.E.; Wijffels, R.H. Phototrophic pigment production with microalgae: Biological constraints and opportunities. *J. Phycol.* **2014**, *50*, 229–242. [CrossRef] [PubMed]
42. Nedaei, L.; Shokrkar, H. Influence of process factors and photobioreactor design on microalgae cultivation. *Biofuels, Bioprod. Biorefin.* **2025**, *19*, 2433–2456. [CrossRef]
43. Nguyen, L.N.; Vu, M.T.; Vu, H.P.; Johir, M.A.H.; Labeeuw, L.; Ralph, P.J.; Mahlia, T.M.I.; Pandey, A.; Sirohi, R.; Nghiem, L.D. Microalgae-based carbon capture and utilization: A critical review on current system developments and biomass utilization. *Crit. Rev. Environ. Sci. Technol.* **2023**, *53*, 216–238. [CrossRef]
44. Nie, C.; Geng, X.; Zhang, R.; Wang, L.; Li, L.; Chen, J. Abundant Cyanobacteria in Autumn Adhering to the Heating, Ventilation, and Air-Conditioning (HVAC) in Shanghai. *Microorganisms* **2023**, *11*, 1835. [CrossRef] [PubMed]
45. Novoveská, L.; Ross, M.E.; Stanley, M.S.; Pradelles, R.; Wasiolek, V.; Sassi, J.F. Microalgal carotenoids: A review of production, current markets, regulations, and future direction. *Mar. Drugs* **2019**, *17*, 640. [CrossRef] [PubMed]
46. Onyeaka, H.; Miri, T.; Obileke, K.C.; Hart, A.; Anumudu, C.; Al-Sharify, Z.T. Minimizing carbon footprint via microalgae as a biological capture. *Carbon Capture Sci. Technol.* **2021**, *1*, 100007. [CrossRef]
47. Pant, S.; Goel, M.; Sahoo, N.K.; Yuan, Q.; Rout, P.R. Microalgae-based treatment for wastewater management and valorization. *Curr. Opin. Environ. Sci. Health* **2025**, *48*, 100662. [CrossRef]
48. Park, J.; Dinh, T.B. Contrasting effects of monochromatic LED lighting on growth, pigments and photosynthesis in the commercially important cyanobacterium *Arthrospira maxima*. *Bioresour. Technol.* **2019**, *291*, 121846. [CrossRef] [PubMed]
49. Pavlov, V.A.; Grigorenko, A.V.; Astafieva, A.P.; Vlaskin, M.S. Growth of Chlorella vulgaris Under Atmospheric CO_2 in Lab-Scale Photobioreactors: Effects of Aeration Rate and Growth Model Comparison. *Bioengineering* **2025**, *12*, 1294. [CrossRef] [PubMed]
50. Pekkoh, J.; Duangjan, K.; Phinyo, K.; Kaewkod, T.; Ruangrit, K.; Thurakit, T.; Pumas, C.; Pathom-aree, W.; Cheirsilp, B.; Gu, W.; et al. Turning waste CO_2 into value-added biorefinery co-products using cyanobacterium *Leptolyngbya* sp. KC45 as a highly efficient living photocatalyst. *Chem. Eng. J.* **2023**, *460*, 141765. [CrossRef]

51. Persily, A.K.; Emmerich, S.J. Indoor air quality in sustainable, energy efficient buildings. *HVAC&R Res.* **2012**, *18*, 4–20. [CrossRef]
52. Quintana, N.; Van Der Kooy, F.; Van De Rhee, M.D.; Voshol, G.P.; Verpoorte, R. Renewable energy from Cyanobacteria: Energy production optimization by metabolic pathway engineering. *Appl. Microbiol. Biotechnol.* **2011**, *91*, 471–490. [CrossRef] [PubMed]
53. Rey-Álvarez, B.; Sánchez-Montañés, B.; Silvestre, E. Harmonizing indoor air quality standards across Europe: A comparative analysis framework for building material regulations and public health protection. *Build. Environ.* **2026**, *288*, 113967. [CrossRef]
54. Salmeron Covarrubias, L.P.; Beluri, K.; Mohammadi, Y.; Easmin, N.; Palacios, O.A.; Sharifan, H. Advanced Nanoenabled Microalgae Systems: Integrating Oxidative Stress-Induced Metabolic Reprogramming and Enhanced Lipid Biosynthesis for Next-Generation Biofuel Production. *ACS Appl. Bio Mater.* **2025**, *8*, 3513–3524. [CrossRef] [PubMed]
55. Singh, N.K.; Sonani, R.R.; Rastogi, R.P.; Madamwar, D. The phycobilisomes: An early requisite for efficient photosynthesis in cyanobacteria. *EXCLI J.* **2015**, *14*, 268. [CrossRef] [PubMed]
56. Song, Y.; Wu, S.; Yan, Y.Y. Control strategies for indoor environment quality and energy efficiency—A review. *Int. J. Low-Carbon Technol.* **2013**, *10*, 305–312. [CrossRef]
57. Sudhakar, K.; Mamat, R. Artificial Leaves: Towards Bio-Inspired Solar Energy Converters. In *Reference Module in Earth Systems and Environmental Sciences*; Elsevier: Amsterdam, The Netherlands, 2019. [CrossRef]
58. Tham, K.W. Indoor air quality and its effects on humans—A review of challenges and developments in the last 30 years. *Energy Build.* **2016**, *130*, 637–650. [CrossRef]
59. Wang, Q.; Li, L.; Hong, Y.; Zhai, Q.; He, Y. Novel insights into indoor air purification capability of microalgae: Characterization using multiple air quality parameters and comparison with common methods. *Environ. Sci. Pollut. Res.* **2023**, *30*, 49829–49839. [CrossRef] [PubMed]
60. Yahaya, E.; Yeo, W.S.; Nandong, J.; Ngu, J.C.Y. CO_2 fed microalgae cultivation in photobioreactor: Review on challenges and possible solutions. *Environ. Technol. Rev.* **2025**, *14*, 540–564. [CrossRef]
61. Yusuf, B.O.; Abdulrasheed, A.A.; Hambali, H.U.; Gbadamosi, A.; Yusuff, A.S.; Afolabi, F.; Aliyu, M.; Ganiyu, S.A. Carbon dioxide (CO_2) capture and utilization technologies: New developments toward net-zero emissions and climate-change mitigation. *Carbon Capture Sci. Technol.* **2026**, *18*, 100589. [CrossRef]
62. Zhou, W.; Wang, J.; Chen, P.; Ji, C.; Kang, Q.; Lu, B.; Li, K.; Liu, J.; Ruan, R. Bio-mitigation of carbon dioxide using microalgal systems: Advances and perspectives. *Renew. Sustain. Energy Rev.* **2017**, *76*, 1163–1175. [CrossRef]

Disclaimer/Publisher's Note: The statements, opinions and data contained in all publications are solely those of the individual author(s) and contributor(s) and not of MDPI and/or the editor(s). MDPI and/or the editor(s) disclaim responsibility for any injury to people or property resulting from any ideas, methods, instructions or products referred to in the content.